

# Analysis of Interdiffused InGaN Quantum Wells for Visible Light-Emitting Diodes

Hongping Zhao, Xuechen Jiao, and Nelson Tansu

**Abstract**—Interdiffused InGaN quantum wells (QWs) with various interdiffusion lengths ( $L_d$ ) are comprehensively studied as the improved active region for Light-Emitting Diodes (LEDs) emitting in the blue and green spectral regime. The electron-hole wavefunction overlap ( $\Gamma_{e-hh}$ ), spontaneous emission spectra, and spontaneous emission radiative recombination rate ( $R_{sp}$ ) for the interdiffused InGaN QWs are calculated and compared to that of the conventional InGaN QWs emitting in the similar wavelengths. The calculations of band structure, confined energy levels, electron and hole wavefunctions, and spontaneous emission radiative recombination rate ( $R_{sp}$ ) are based on the self-consistent 6-band  $k \cdot p$  method, taking into account the valence band mixing, strain effect, spontaneous and piezoelectric polarizations and carrier screening effect. Studies indicate a significant enhancement of the electron-hole wavefunction overlap ( $\Gamma_{e-hh}$ ) and the spontaneous emission radiative recombination rate ( $R_{sp}$ ) for the interdiffused InGaN QWs. The improved performance for the interdiffused InGaN QWs is due to the modification of the band lineups at the InGaN-GaN interfaces, which leads to the enhancement of the electron-hole wavefunction overlap significantly.

**Index Terms**—InGaN quantum wells (QWs), light-emitting diodes (LEDs), interdiffusion.

## I. INTRODUCTION

III-NITRIDE semiconductor based quantum wells (QWs) as active region for light-emitting-diodes (LEDs) and laser diodes (LDs) with emission wavelength in the visible and near ultraviolet spectral regimes attract increasing interest [1]–[5]. Particularly, the ternary InGaN QWs are widely used in blue- and green-emitting LEDs, which have great potential to serve as the next-generation illumination devices [6]–[10]. However, it is still challenging to achieve high performance InGaN QWs, especially in the green and longer wavelength region, due to: 1) high threading dislocation densities in InGaN QWs, originating from the lacking of lattice-matched substrate; 2) phase separation in high-In content InGaN QWs; and 3) severe charge separation due to the existence of internal electrostatic field in c-plane InGaN QWs. InGaN QWs grown along c-plane sapphire substrate contain

both spontaneous and piezoelectric polarizations, which induces significant reduction of the electron-hole wavefunction overlap ( $\Gamma_{e-hh}$ ) in InGaN QWs [11]. In order to extend the emission wavelength of InGaN QWs toward green and longer wavelength, InGaN QWs with higher In-content and wider QW thickness are needed, both of which lead to larger electrostatic field in InGaN QW and more severe charge separation. This results in significant reduction of electron-hole wavefunction overlap ( $\Gamma_{e-hh}$ ) and reduction of the internal quantum efficiency [12].

Recently, several approaches have been proposed to suppress the charge separation issue and enhance the electron-hole wavefunction overlap ( $\Gamma_{e-hh}$ ) in c-plane InGaN QWs by using the large overlap QW design such as: 1) staggered InGaN QW [8], [12]–[16], 2) type-II InGaN-GaNAs QW [17]–[19], 3) InGaN QW with  $\delta$ -AlGaIn layer [20], [21], 4) strain-compensated InGaN-AlGaIn QW [22], 5) InGaN-delta-InN QW [23], [24]. The purpose of using these novel quantum well designs is to enhance the electron-hole wavefunction overlap ( $\Gamma_{e-hh}$ ) and thus to improve the spontaneous emission radiative recombination rate ( $R_{sp}$ ) via engineering the energy band lineups of InGaN QWs.

In this study, we performed the comprehensive studies of the interdiffused InGaN QWs [25]–[27]. The optical properties of the interdiffused InGaN QWs emitting in both blue and green spectral regimes with various interdiffusion lengths ( $L_d$ ) were compared to that of the conventional InGaN QWs. Note that the approach based on the novel QW designs requires modifications and optimizations of the epitaxial recipe of the InGaN QWs in order to grow different types of QWs [12]–[23]. In contrast, interdiffusion based on rapid thermal annealing (RTA) approach is a post-growth procedure for engineering the QW shapes widely implemented in InGaAs/GaAs heterostructures [28]–[30], which avoids the need for modification in the epitaxial recipe for lasers and LEDs.

## II. IN/GA INTERDIFFUSION IN INGAN QWS

Interdiffusion based on RTA is a cost-effective approach to improve the optical and electrical properties of as-grown InGaN/GaN QWs, especially for the InGaN QWs with high-In content [31]. During the rapid thermal annealing process, the interdiffusion of indium (In) and gallium (Ga) atoms at the interface of InGaN QW and GaN barrier takes place, where indium atoms in InGaN QW diffuse into GaN barrier region and gallium atoms in GaN layer diffuse into InGaN QW region. The interdiffusion of indium and gallium between InGaN QWs and GaN barriers significantly modifies the energy band lineups for InGaN QWs, which leads to the shift of both electron and hole wavefunctions, resulting in enhancement of the electron-hole wavefunction overlap ( $\Gamma_{e-hh}$ ). Note that the

Manuscript received January 20, 2013; revised February 09, 2013, February 26, 2013; accepted February 27, 2013. Date of publication March 11, 2013; date of current version March 15, 2013. This work was supported by the Case Western Reserve University Start-Up Fund (H.Z.), and by the U.S. National Science Foundation under ECCS-1028490 (N.T.).

H. Zhao and X. Jiao are with the Department of Electrical Engineering and Computer Science, Case Western Reserve University, Cleveland, OH 44106 USA (e-mail: hongping.zhao@case.edu).

N. Tansu is with the Center for Photonics and Nanoelectronics, Department of Electrical and Computer Engineering, Lehigh University, Bethlehem, PA 18015 USA (e-mail: tansu@lehigh.edu).

Color versions of one or more of the figures are available online at <http://ieeexplore.ieee.org>.

Digital Object Identifier 10.1109/JDT.2013.2250480

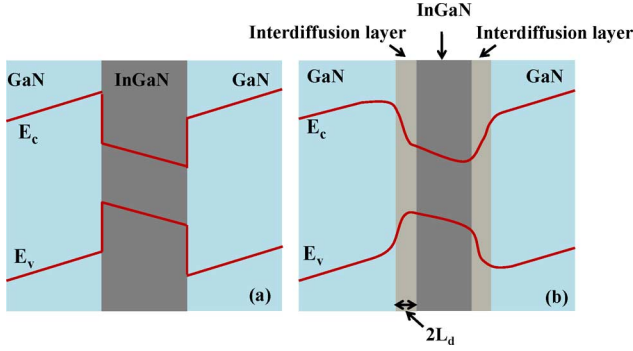


Fig. 1. Schematics for (a) the conventional 3-nm  $\text{In}_{0.25}\text{Ga}_{0.75}$  QWs and (b) the interdiffused 3-nm  $\text{In}_{0.25}\text{Ga}_{0.75}$  QWs with interdiffusion length  $L_d = 5$  Å.

interdiffusion length ( $L_d$ ) has a significant effect on the energy band lineups, which could be controlled via the rapid thermal annealing condition [27].

Fig. 1 plots the schematics of (a) the conventional InGaN QW and (b) the interdiffused InGaN QW structures, both of which are surrounded by GaN barrier layers. From Fig. 1(a), the conventional InGaN QW contains uniform indium content across the whole InGaN QW region, resulting in sharp energy band lineups at the InGaN/GaN interfaces. From Fig. 1(b), the interdiffused InGaN QW contains an error-function like indium content profile at the InGaN/GaN interfaces [25], resulting in smooth energy band lineups at the InGaN/GaN interfaces. The thickness of the transition layer (as shown in Fig. 1(b)) is defined as two times of the interdiffusion length ( $L_d$ ). Note that the interdiffusion length could be engineered by controlling the RTA conditions such as the RTA temperature, the RTA duration, and the RTA ambient [27].

The smooth energy band lineups for the interdiffused InGaN QWs push the electron and hole wavefunctions toward the center of the QW region, resulting in enhanced electron-hole wavefunction overlap ( $\Gamma_{e\text{-}hh}$ ). According to Fermi's Golden Rule, the rate of interband transition is proportional to the square of electron-hole wavefunction overlap ( $|\Gamma_{e\text{-}hh}|^2$ ) [32]. Thus, the interdiffused InGaN QWs are expected to show higher spontaneous emission radiative recombination rate ( $R_{\text{sp}}$ ) than that of conventional InGaN QWs.

### III. SIMULATION METHOD

The calculation of the energy band structure of the InGaN QWs is based on a self-consistent 6-band  $\mathbf{k} \cdot \mathbf{p}$  method for wurtzite semiconductors [22], [32], [33]. In the calculation, the model takes into account the valance band mixing, strain effect, spontaneous and piezoelectric polarizations, and carrier screening effect [22]. The coupling between the conduction band and valance band is negligible and not considered here, as the band gap in InGaN QW is relatively large. The calculation of the spontaneous emission radiative recombination rate ( $R_{\text{sp}}$ ) in InGaN QWs includes both transverse electric (TE) and transverse magnetic (TM) polarization components, and it is obtained by averaging the momentum matrix elements of TE polarization ( $|M_{\text{TE}}|^2$ ) and TM polarization ( $|M_{\text{TM}}|^2$ ) as  $|M_{\text{sp}}|^2 = (2|M_{\text{TE}}|^2 + |M_{\text{TM}}|^2)/3$ . The details of the simula-

tion model including band parameters and material properties are based on the data used in [22], [32], and [33].

The parameters involved in the calculation of optical properties for InGaN QWs were obtained from other [34]. For the ternary  $\text{In}_x\text{Ga}_{1-x}\text{N}$  alloy, the corresponding parameters can be calculated by the linear interpolation of parameters from GaN and InN, except for the energy band gap  $E_g$ , which can be expressed as:  $E_g(\text{In}_x\text{Ga}_{1-x}\text{N}) = x \cdot E_g(\text{InN}) + (1-x) \cdot E_g(\text{GaN}) - b \cdot x \cdot (1-x)$ . Note that the bowing parameter  $b$  is set as 1.4 eV [34], the band offset ratio ( $\Delta E_c : \Delta E_v$ ) of InGaN/GaN is set as 0.7:0.3 in our calculation.

For the interdiffused InGaN QWs, the indium content profile at the GaN-InGaN-GaN interfaces is determined by Fick's Law [35], as follow:

$$C(z) = \frac{1}{2}C_0 \left[ \text{erf} \left( \frac{h-z}{L_d} \right) + \text{erf} \left( \frac{h+z}{L_d} \right) \right] \quad (1)$$

where  $C_0$  is the initial indium content,  $h$  is the QW width,  $z$  is the coordinate along the crystal growth direction and  $L_d$  is the diffusion length. Note that the diffusion length  $L_d$  is determined by both temperature and material properties [36]. The diffusion lengths and coefficients for In/Ga atoms across InGaN interface had been reported in [36]. The diffusion coefficient for In/Ga atoms at InGaN interface [36] was found to follow Arrhenius expression as  $D = 1.93 \times 10^{11} \exp(-40473/T) \text{ \AA}^2/\text{sec}$ , where  $T$  represents temperature in K. The diffusion length  $L_d$  is related to the diffusion coefficient  $D$  by the following relation  $L_d = 2\sqrt{D \cdot t}$ , where  $t$  represents the time of diffusion.

The spontaneous emission spectra can be obtained by taking into account all the transitions between the  $n$ th conduction subband and the  $m$ th valance subband as follow [22], [29], [33]:

$$r^{\text{spon}}(\hbar\omega) = \frac{2q^2\pi}{n_r c \epsilon_0 m_0^2 \omega L_w} \sum_{\sigma=U,L} \sum_{n,m} \int \frac{k_t dk_t}{2\pi} |(M)_{nm}(k_t)|^2 \times \frac{f_n^c(k_t)(1-f_{\sigma m}^v(k_t))(\gamma/\pi)}{(E_{\sigma, nm}^{cv}(k_t) - \hbar\omega)^2 + \gamma^2} \quad (2)$$

where  $f_n^c(k_t)$  and  $f_{\sigma m}^v(k_t)$  are the Fermi-Dirac distribution functions for the electrons in conduction band and holes in valance band,  $k_t$  is the in-plane wave vector,  $L_w$  is the thickness of the QW,  $(M)_{nm}(k_t)$  is the momentum matrix element between the  $n$ th conduction subband and the  $m$ th valance subband. Because of the lacking of symmetry of the energy band lineups for the conduction band and valance band, the transitions between states with unequal quantum numbers ( $m \neq n$ ) are not zero. In the simulation, all possible transitions between the confined states of the  $n$ th conduction subbands and  $m$ th valance subbands are taken into account.

To investigate the improvement of the optical properties for the interdiffused InGaN QWs, the spontaneous emission radiative recombination rate ( $R_{\text{sp}}$ ) is calculated by integrating the (2) over the entire frequency range as follow:

$$R_{\text{sp}} = \int_0^\infty r^{\text{spon}}(\hbar\omega) d(\hbar\omega). \quad (3)$$

### IV. SIMULATION RESULTS

In this study, we performed the optimization studies of the interdiffused InGaN/GaN QWs emitting in blue and green spec-

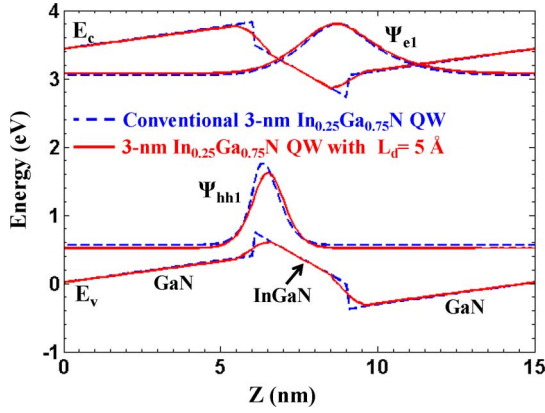


Fig. 2. Energy band lineups and wavefunctions of electron and hole for the conventional 3-nm  $\text{In}_{0.25}\text{Ga}_{0.75}\text{N}$  QWs (blue dash line) and the interdiffused 3-nm  $\text{In}_{0.25}\text{Ga}_{0.75}\text{N}$  QWs with  $L_d = 5 \text{ \AA}$  (red solid line).

tral regimes, respectively. In the blue (green) regime, the optical properties of 3-nm  $\text{In}_{0.25}\text{Ga}_{0.75}\text{N}$  (3.5-nm  $\text{In}_{0.3}\text{Ga}_{0.7}\text{N}$ ) QWs with various interdiffusion length ( $L_d$ ) from 1  $\text{\AA}$  to 10  $\text{\AA}$  are simulated, as compared to that of the conventional 3-nm  $\text{In}_x\text{Ga}_{1-x}\text{N}$  (3.5-nm  $\text{In}_x\text{Ga}_{1-x}\text{N}$ ) QWs emitting at the similar emission wavelength. The effects of the interdiffusion lengths  $L_d$  on 1) the inter-band transition wavelengths, 2) spontaneous emission radiative recombination rates were comprehensively studied.

Note that the engineering of interdiffusion length  $L_d$  can be realized by modifying the annealing temperature and duration. To illustrate the experimental method, the choice of  $L_d = 5 \text{ \AA}$  can be realized by employing post growth annealing at 1000 $^\circ\text{C}$  for a duration of 30 minutes [27]. By using post growth annealing temperature of 950 $^\circ\text{C}$  for a duration of 40 minutes, the interdiffusion length of  $L_d = 5 \text{ \AA}$  can be achieved [27].

#### A. Interdiffused Blue InGaN QWs

Fig. 2 shows the energy band lineups of the conventional 3-nm  $\text{In}_{0.25}\text{Ga}_{0.75}\text{N}$  QW (blue dash lines) and the interdiffused 3-nm  $\text{In}_{0.25}\text{Ga}_{0.75}\text{N}$  QW with interdiffusion length of  $L_d = 5 \text{ \AA}$  (red solid lines). The interdiffusion of indium and gallium atoms across the InGaN/GaN interfaces leads to the modification of the band lineups, which in turn results in smooth interfaces between InGaN and GaN layers. The corresponding electron and hole wavefunctions for the first confined conduction subband (EC1) and first confined valence subband (HH1) were plotted. From Fig. 2, the electron and hole wavefunctions of the interdiffused InGaN QW shift toward the center of the QW region which leads to the enhancement of the electron-hole wavefunction overlap ( $\Gamma_{e,hh}$ ) from 17.3% to 22.1%.

In addition to the enhanced electron-hole wavefunction overlap ( $\Gamma_{e,hh}$ ) for the interdiffused InGaN QWs, the effect of the band lineups modification leads to the shift of the confined energy levels in both conduction band and valence band, which results in the shift of the interband transition wavelength. Fig. 3 shows the confined energy levels (EC2, EC1, HH1, LH1, HH2 and LH2) as a function of the interdiffusion length ( $L_d$ ). With the increase of interdiffusion length ( $L_d$ ), both conduction and valence band confined energy levels increase, which leads to

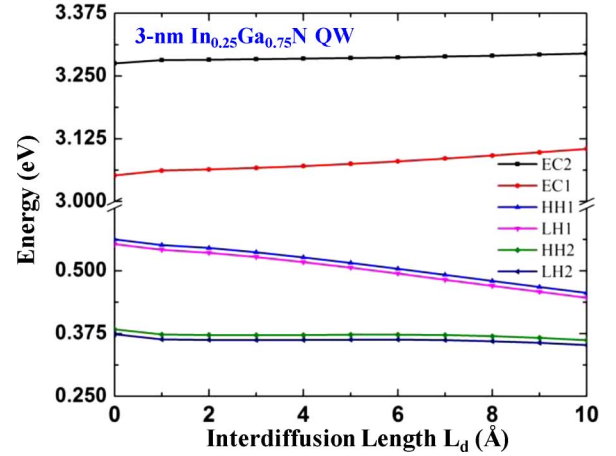


Fig. 3. Confined energy states of the conduction bands (EC1 and EC2) and the valence bands (HH1, LH1, HH2 and LH2) for interdiffused 3-nm  $\text{In}_{0.25}\text{Ga}_{0.75}\text{N}$  QWs as a function of interdiffusion length  $L_d$ .

the blue-shift of the peak emission wavelength ( $\lambda_{\text{peak}}$ ). Note that as  $L_d$  increases, the lower confined energy levels (EC1, HH1/LH1) increase more obviously as compared to the high energy levels (EC2, HH2/LH2, etc.). The transition wavelength between conduction band and valence band is determined dominantly by the lower energy levels (EC1, HH1/LH1) for LED application with low current injection. For 3-nm  $\text{In}_{0.25}\text{Ga}_{0.75}\text{N}$  QW, the peak emission wavelength ( $\lambda_{\text{peak}}$ ) blue-shifts from 495 nm for conventional InGaN QW ( $L_d = 0 \text{ \AA}$ ) to 465 nm for interdiffused InGaN QW ( $L_d = 10 \text{ \AA}$ ).

In order to compare the optical performance of the interdiffused InGaN QWs with that of the conventional InGaN QWs emitting at the similar emission wavelength, Fig. 4 plots the electron-hole wavefunction overlap ( $\Gamma_{e,hh}$ ) for the interdiffused 3-nm  $\text{In}_{0.25}\text{Ga}_{0.75}\text{N}$  QWs (with  $L_d = 0 \text{ \AA}$  up to  $L_d = 10 \text{ \AA}$ ) and the conventional 3-nm  $\text{In}_x\text{Ga}_{1-x}\text{N}$  QWs (with  $x = 0.25$  to  $x = 0.215$ ) as a function of peak emission wavelength ( $\lambda_{\text{peak}}$ ). It is observed that the overlap  $\Gamma_{e,hh}$  for the conventional 3-nm  $\text{In}_x\text{Ga}_{1-x}\text{N}$  QWs increases from 17.3% to 21% as the peak emission wavelength  $\lambda_{\text{peak}}$  decreases from 495 nm ( $x = 0.25$ ) to 465 nm ( $x = 0.215$ ), which is due to the reduction of the electrostatic field in the InGaN QW with decrease of the In-content. While for the interdiffused 3-nm  $\text{In}_{0.25}\text{Ga}_{0.75}\text{N}$  QWs, the overlap  $\Gamma_{e,hh}$  is enhanced from 17.3% to 24.5% with the increase of interdiffusion length ( $L_d$ ) from  $L_d = 0 \text{ \AA}$  to  $L_d = 10 \text{ \AA}$ , corresponding to the decrease of the peak emission wavelength  $\lambda_{\text{peak}}$  from 495 nm to 465 nm. From Fig. 4, the interdiffused 3-nm  $\text{In}_{0.25}\text{Ga}_{0.75}\text{N}$  QWs show enhanced electron-hole wavefunction overlap ( $\Gamma_{e,hh}$ ) as compared to that of the conventional 3-nm  $\text{In}_x\text{Ga}_{1-x}\text{N}$  QWs emitting at the same peak emission wavelength.

The spontaneous emission radiative recombination rate ( $R_{\text{sp}}$ ) for the interdiffused 3-nm  $\text{In}_{0.25}\text{Ga}_{0.75}\text{N}$  QWs with various interdiffusion length ( $L_d$ ) are calculated as compared to that of the conventional 3-nm  $\text{In}_x\text{Ga}_{1-x}\text{N}$  QWs with different In-contents ( $x$ ). Note that the conventional 3-nm  $\text{In}_x\text{Ga}_{1-x}\text{N}$  QWs are designed such that the peak emission wavelengths are similar to that of the interdiffused 3-nm  $\text{In}_{0.25}\text{Ga}_{0.75}\text{N}$  QWs. The calculated spontaneous emission spectra for both structures are

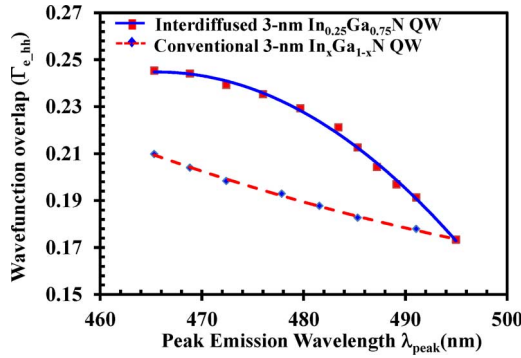


Fig. 4. Electron-hole wavefunction overlap ( $\Gamma_{e,h}$ ) for the conventional 3-nm  $\text{In}_x\text{Ga}_{1-x}\text{N}$  QWs and the interdiffused 3-nm  $\text{In}_{0.25}\text{Ga}_{0.75}\text{N}$  QWs as a function of peak emission wavelength ( $\lambda_{peak}$ ).

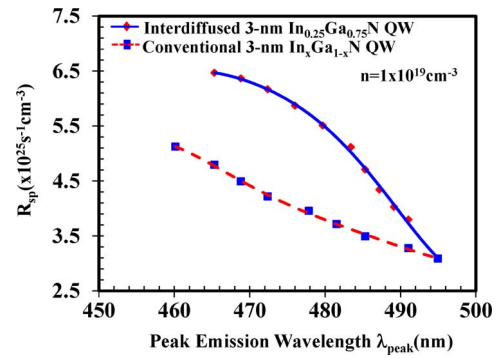


Fig. 6. Spontaneous emission radiative recombination rate ( $R_{sp}$ ) for the conventional 3-nm  $\text{In}_{0.25}\text{Ga}_{0.75}\text{N}$  QWs and the interdiffused 3-nm  $\text{In}_{0.25}\text{Ga}_{0.75}\text{N}$  QWs as a function of peak emission wavelength ( $\lambda_{peak}$ ).

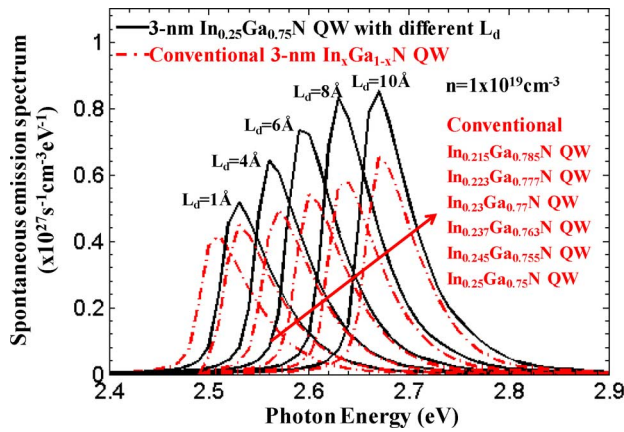


Fig. 5. Spontaneous emission spectra for the conventional 3-nm  $\text{In}_{0.25}\text{Ga}_{0.75}\text{N}$  QWs and the interdiffused 3-nm  $\text{In}_{0.25}\text{Ga}_{0.75}\text{N}$  QWs at  $T = 300 \text{ K}$  and charge density  $n = 10 \times 10^{18} \text{ cm}^{-3}$ .

shown in Fig. 5 with carrier density  $n = 1 \times 10^{19} \text{ cm}^{-3}$  and temperature  $T = 300 \text{ K}$ .

From Fig. 5, the spontaneous emission spectra of the interdiffused 3-nm  $\text{In}_{0.25}\text{Ga}_{0.75}\text{N}$  QWs are significantly enhanced as compared to that of the conventional 3-nm  $\text{In}_x\text{Ga}_{1-x}\text{N}$  QWs emitting at the similar peak emission wavelength  $\lambda_{peak}$ . For the conventional 3-nm  $\text{In}_x\text{Ga}_{1-x}\text{N}$  QWs, the spontaneous emission radiative recombination intensities increase as the peak emission wavelength  $\lambda_{peak}$  blue-shifts with the decrease of In-content  $x$ . While for the interdiffused 3-nm  $\text{In}_{0.25}\text{Ga}_{0.75}\text{N}$  QWs, the spontaneous emission radiative recombination intensities increase as the peak emission wavelength  $\lambda_{peak}$  blue-shifts with the increase of interdiffusion length ( $L_d$ ).

Fig. 6 shows the spontaneous emission radiative recombination rate ( $R_{sp}$ ) for both the interdiffused 3-nm  $\text{In}_{0.25}\text{Ga}_{0.75}\text{N}$  QWs and the conventional 3-nm  $\text{In}_x\text{Ga}_{1-x}\text{N}$  QWs as a function of the peak emission wavelength ( $\lambda_{peak}$ ). The spontaneous emission radiative recombination rate ( $R_{sp}$ ) for both QW structures increase with the blue-shift of the peak emission wavelength ( $\lambda_{peak}$ ) in the blue spectral regime. The interdiffused 3-nm  $\text{In}_{0.25}\text{Ga}_{0.75}\text{N}$  QWs shows higher  $R_{sp}$  than that of the conventional 3-nm  $\text{In}_x\text{Ga}_{1-x}\text{N}$  QWs at the similar peak emission wavelength ( $\lambda_{peak}$ ). For example, at the peak emission wavelength  $\lambda_{peak} = 470 \text{ nm}$ , the  $R_{sp}$  of the interdiffused 3-nm  $\text{In}_{0.25}\text{Ga}_{0.75}\text{N}$  QWs (with  $L_d = 8 \text{ \AA}$ ) is  $6.3 \times 10^{25} \text{ s}^{-1} \text{ cm}^{-3}$ ,

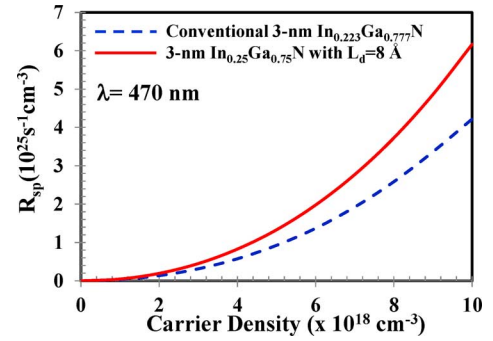


Fig. 7. The spontaneous emission radiative recombination rate ( $R_{sp}$ ) as a function of charge density in blue spectral region.

while the  $R_{sp}$  of conventional 3-nm  $\text{In}_x\text{Ga}_{1-x}\text{N}$  QWs (with  $x = 0.22$ ) is  $4.5 \times 10^{25} \text{ s}^{-1} \text{ cm}^{-3}$ , indicating an improvement of  $\sim 1.4$  times.

Fig. 7 shows the comparison of the  $R_{sp}$  for the conventional 3-nm  $\text{In}_{0.223}\text{Ga}_{0.777}\text{N}$  QWs and the interdiffused 3-nm  $\text{In}_{0.25}\text{Ga}_{0.75}\text{N}$  QWs with  $L_d = 8 \text{ \AA}$  as a function of the carrier density ( $n = 0-1 \times 10^{19} \text{ cm}^{-3}$ ). Both QWs emit at the peak emission wavelength  $\lambda_{peak}$  of 470 nm. From Fig. 7, the  $R_{sp}$  of both 3-nm  $\text{In}_{0.223}\text{Ga}_{0.777}\text{N}$  QWs and 3-nm  $\text{In}_{0.25}\text{Ga}_{0.75}\text{N}$  QWs with  $L_d = 8 \text{ \AA}$  increase with the increase of the carrier density. The interdiffused InGaN QW shows enhanced  $R_{sp}$  at different carrier density as compared to that of the conventional InGaN QW. The enhancement of the  $R_{sp}$  for the interdiffused InGaN QWs is due to the engineered energy band lineups with smooth transition layer at the InGaN/GaN interfaces, which leads to the shift of the electron and hole wavefunctions with enhanced electron-hole wavefunction overlap.

The simulation results from this study show the similar trend as the experimental results [27], [36]. As the diffusion length  $L_d$  increases, the interband transition wavelength blue-shifts accompanied by the increase in the spontaneous emission radiative recombination rate.

### B. Interdiffused Green InGaN QWs

As compared to the blue-emitting InGaN QWs, it is more challenging to achieve high performance green InGaN QWs due to the requirement of thick QW and relatively high In-content for the InGaN QWs [12]. The interdiffused InGaN QWs emitting in the green spectral region are analyzed as improved

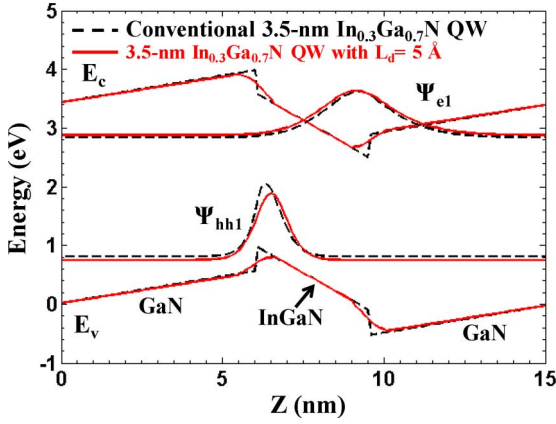


Fig. 8. Schematics for (a) the conventional 3.5-nm  $\text{In}_{0.3}\text{Ga}_{0.7}\text{N}$  QWs and (b) the interdiffused 3.5-nm  $\text{In}_{0.3}\text{Ga}_{0.7}\text{N}$  QWs with interdiffusion length  $L_d = 5 \text{ \AA}$ .

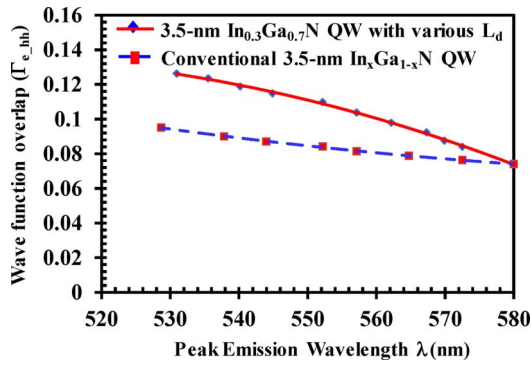


Fig. 9. Electron-hole wavefunction overlap ( $\Gamma_{e-hh}$ ) for the conventional 3.5-nm  $\text{In}_x\text{Ga}_{1-x}\text{N}$  QWs and the interdiffused 3.5-nm  $\text{In}_{0.3}\text{Ga}_{0.7}\text{N}$  QWs as a function of peak emission wavelength ( $\lambda_{\text{peak}}$ ).

QWs with enhanced electron-hole wavefunction overlap. Specifically, the following two structures are calculated and compared: 1) the conventional 3.5-nm  $\text{In}_x\text{Ga}_{1-x}\text{N}$  QWs with various In-content ( $x$ ); and 2) the interdiffused 3.5-nm  $\text{In}_{0.3}\text{Ga}_{0.7}\text{N}$  QWs with various interdiffusion lengths ( $L_d$ ).

Fig. 8 plots the energy band lineups and electron and hole wavefunctions for the conventional 3.5-nm  $\text{In}_{0.3}\text{Ga}_{0.7}\text{N}$  QW (black dash line) and the interdiffused 3.5-nm  $\text{In}_{0.3}\text{Ga}_{0.7}\text{N}$  QW with interdiffusion length of  $L_d = 5 \text{ \AA}$  (red solid line). Similar to the blue-emitting InGaN QWs, the step-function like energy band lineups for the conventional 3.5-nm  $\text{In}_{0.3}\text{Ga}_{0.7}\text{N}$  QW are transformed to error-function like band lineups for the interdiffused InGaN QW, which pushes the electron and hole wavefunctions toward the center of the QW, resulting in enhanced electron-hole wavefunction overlap ( $\Gamma_{e-hh}$ ).

Fig. 9 shows the electron-hole wavefunction overlap ( $\Gamma_{e-hh}$ ) for the conventional 3.5-nm  $\text{In}_x\text{Ga}_{1-x}\text{N}$  QWs and the interdiffused 3.5-nm  $\text{In}_{0.3}\text{Ga}_{0.7}\text{N}$  QWs emitting in the green spectral region as a function of the peak emission wavelength ( $\lambda_{\text{peak}}$ ). We observe a significant enhancement of the overlap  $\Gamma_{e-hh}$  for the interdiffused InGaN QW compared to that of the conventional one as the blue-shift of the peak emission wavelength ( $\lambda_{\text{peak}}$ ). At  $\lambda_{\text{peak}} = 540 \text{ nm}$ , the  $\Gamma_{e-hh}$  is enhanced by 1.33 times for the interdiffused InGaN QW as compared to that of the

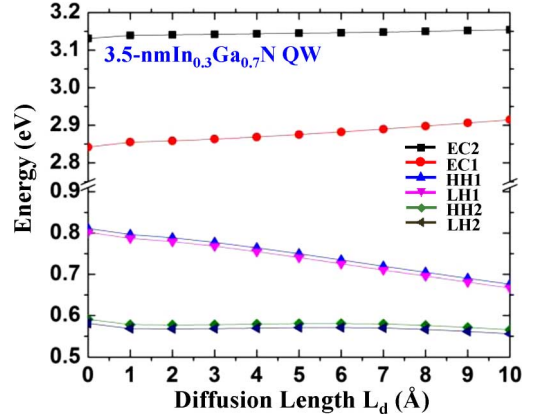


Fig. 10. Confined energy states of the conduction bands (EC1 and EC2) and the valance bands (HH1, LH1, HH2 and LH2) for interdiffused 3.5-nm  $\text{In}_{0.3}\text{Ga}_{0.7}\text{N}$  QWs as a function of interdiffusion length  $L_d$ .

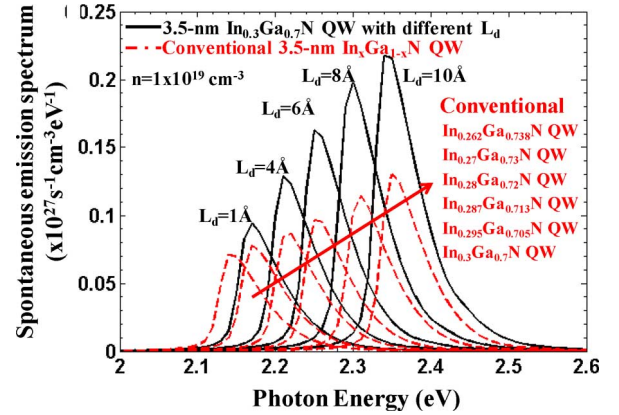


Fig. 11. Spontaneous emission spectra for the conventional 3.5-nm  $\text{In}_{0.3}\text{Ga}_{0.7}\text{N}$  QWs and the interdiffused 3.5-nm  $\text{In}_{0.3}\text{Ga}_{0.7}\text{N}$  QWs at  $T = 300 \text{ K}$  and charge density  $n = 10 \times 10^{18} \text{ cm}^{-3}$ .

conventional one. Fig. 10 plots the confined energy states (EC1, EC2, HH1, LH1, HH2 and LH2) for the interdiffused 3.5-nm  $\text{In}_{0.3}\text{Ga}_{0.7}\text{N}$  QWs as a function of the interdiffusion length ( $L_d$ ) from  $0 \text{ \AA}$  to  $10 \text{ \AA}$ . As the interdiffusion length ( $L_d$ ) increases, both EC1 and HH1/LH1 (absolute value) increase significantly, which leads to a strong blue-shift of the transition wavelength for interdiffused 3.5-nm  $\text{In}_{0.3}\text{Ga}_{0.7}\text{N}$  QWs.

Fig. 11 shows the comparison of the spontaneous emission spectra between the interdiffused 3.5-nm  $\text{In}_{0.3}\text{Ga}_{0.7}\text{N}$  QWs and the conventional 3.5-nm  $\text{In}_x\text{Ga}_{1-x}\text{N}$  QWs emitting in green spectral region. As the blue-shift of the peak emission wavelength, both interdiffused and conventional QWs show increase in spontaneous emission spectra. Yet the interdiffused InGaN QWs show stronger enhancement as compared to that of the conventional one. This indicates that the interdiffusion allows a significant enhancement of the spontaneous emission radiative recombination rate for the InGaN QWs emitting in the green spectral region. To illustrate this more clearly, Fig. 12 plots the spontaneous emission radiative recombination rate  $R_{\text{sp}}$  of the interdiffused InGaN QW and the conventional one as a function of the peak emission wavelength. The  $R_{\text{sp}}$  of the interdiffused InGaN QW increases more rapidly as compared to that of the

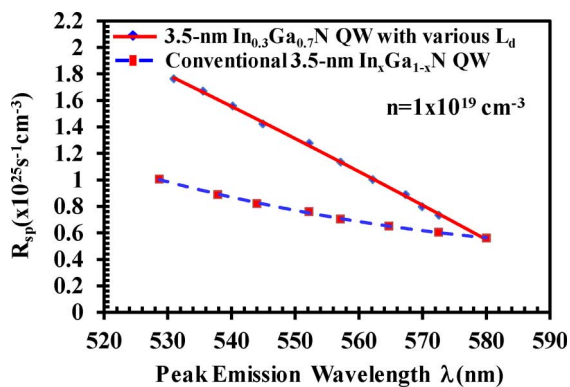


Fig. 12. Spontaneous emission radiative recombination rate ( $R_{sp}$ ) for the conventional 3.5-nm  $\text{In}_{0.3}\text{Ga}_{0.7}\text{N}$  QWs and the interdiffused 3.5-nm  $\text{In}_{0.3}\text{Ga}_{0.7}\text{N}$  QWs as a function of peak emission wavelength ( $\lambda_{peak}$ ).

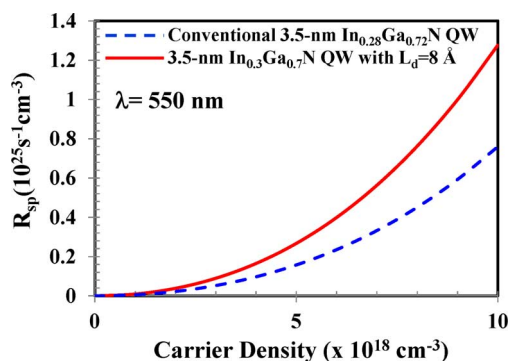


Fig. 13. The spontaneous emission radiative recombination rate ( $R_{sp}$ ) as a function of charge density in green spectral region.

the conventional InGaN QW as the emission wavelength getting shorter.

Fig. 13 shows the comparison of the  $R_{sp}$  of the interdiffused 3.5-nm  $\text{In}_{0.3}\text{Ga}_{0.7}\text{N}$  QWs with  $L_d = 6 \text{ \AA}$  and the conventional 3.5-nm  $\text{In}_{0.28}\text{Ga}_{0.72}\text{N}$  QWs emitting at 550 nm as a function of the carrier density up to  $1 \times 10^{19} \text{ cm}^{-3}$ . The interdiffused InGaN QW shows improved  $R_{sp}$  at different carrier densities.

### C. Blue and Green Interdiffused InGaN QWs

In order to compare the optical performances for the interdiffused InGaN QWs emitting at blue and green spectral regimes, Fig. 14 plots the  $R_{sp}$  ratio of the interdiffused and conventional InGaN QWs for both blue [Fig. 14(a)] and green [Fig. 14(b)] wavelength regimes.

In the blue emission, the interdiffused InGaN QW shows enhancement of the  $R_{sp}$  as the wavelength shortens. The enhancement ratio increases from 1.1 times at 494 nm to 1.5 times at 475 nm. Note that the ratio reaches its peak at around 475 nm, which indicates there is an optimized interdiffusion length for the blue-emitting InGaN QWs. In the green emission, the interdiffused InGaN QW shows monotonically increase of the  $R_{sp}$  ratio as the emission wavelength shortens. The enhancement ratio increases from 1.2 times at 574 nm to 1.8 times at 533 nm. This indicates that the interdiffusion is an effective approach to enhance the optical performance for both blue

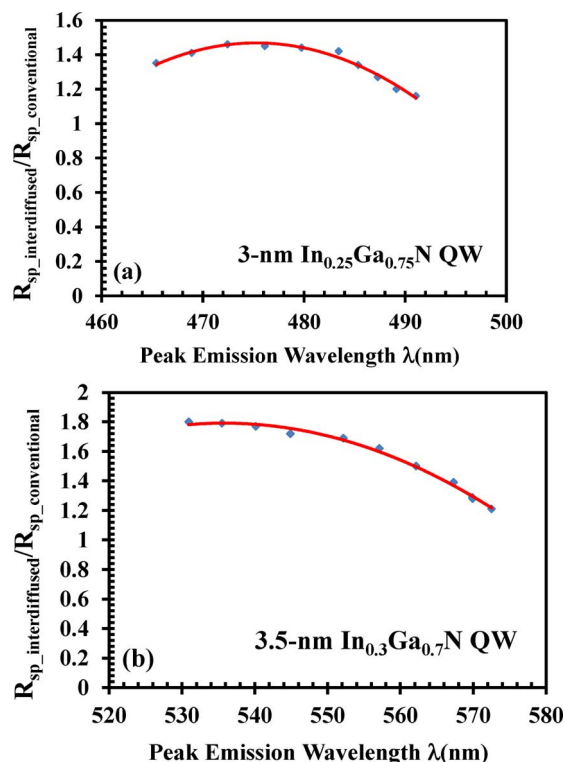


Fig. 14. The  $R_{sp}$  ratio of interdiffused InGaN QWs over the conventional InGaN QWs in (a) the blue spectral regime and (b) green spectral regime.

and green emitting InGaN QWs. The enhancement is more significant for the green-emitting InGaN QWs with high In-content and thick QW. Thus, interdiffusion has great potential to serve as a cost-effective approach to enhance the performance for InGaN QWs LEDs, especially emitting at green and longer wavelength regimes.

## V. SUMMARY

In summary, the interdiffused InGaN QWs emitting in both blue and green spectral regimes are comprehensively analyzed. With the error-function like interface band lineups, the interdiffused InGaN QWs show enhanced electron-hole wavefunction overlap as compare to that of the conventional InGaN QWs emitting at similar wavelength. The interdiffusion, which is achievable by rapid thermal annealing, provides a cost-effective approach to engineer the QW band structures for enhancing the QW performance, which has great potential to achieve InGaN QW based LEDs with improved radiative recombination rate and radiative efficiency emitting applicable for solid state lighting.

## REFERENCES

- [1] M. H. Crawford, "LEDs for solid-state lighting: Performance challenges and recent advances," *IEEE J. Sel. Top. Quantum Electron.*, vol. 15, no. 4, pp. 1028–1040, July/Aug. 2009.
- [2] D. Queren, A. Avramescu, G. Bruderl, A. Breidenassel, M. Schillgales, S. Lutgen, and U. Strauß, "500 nm electrically driven InGaN based laser diodes," *Appl. Phys. Lett.*, vol. 94, no. 8, p. 081119, Feb. 2009.

- [3] N. Tansu, H. Zhao, G. Liu, X. H. Li, J. Zhang, H. Tong, and Y. K. Ee, "III-nitride photonics," *IEEE Photonics J.*, vol. 2, no. 2, pp. 241–248, Apr. 2010.
- [4] S. Chichibu, T. Azuhata, T. Sota, and S. Nakamura, "Spontaneous emission of localized excitons in InGaN single and multi-quantum well structures," *Appl. Phys. Lett.*, vol. 69, no. 27, pp. 4188–4190, Oct. 1996.
- [5] G. R. Mutta, P. Ruterana, J. L. Doualan, M. P. Chauvat, F. Ivaldi, S. Kret, N. A. K. Kaufmann, A. Dussaigne, D. Martin, and N. Grandjean, "Investigation of the In composition in InGaN/GaN quantum wells deposited by MOVPE and/or MBE with emission from violet to green," *Phys. Status Solidi (B)*, vol. 248, no. 5, pp. 1187–1190, May 2011.
- [6] J. Zhang, J. Yang, G. Simin, M. A. Shatalov, M. A. Khan, M. S. Shur, and R. Gaska, "Enhanced luminescence in InGaN multiple quantum wells with quaternary AlInGaN barriers," *Appl. Phys. Lett.*, vol. 77, no. 17, pp. 2668–2670, Oct. 2000.
- [7] S. Nakamura, M. Senoh, N. Iwasa, S. Nagahama, T. Yamada, and T. Mukai, "Superbright green InGaN single-quantum-well-structure light-emitting diodes," *Jpn. J. Appl. Phys.*, vol. 34, no. 10B, pp. L1332–L1335, Oct. 1995, Part 2.
- [8] H. Zhao, G. Liu, J. Zhang, J. D. Poplawsky, V. Dierolf, and N. Tansu, "Approaches for high internal quantum efficiency green InGaN light-emitting diodes with large overlap quantum wells," *Opt. Express*, vol. 19, no. 54, pp. A991–A1007, Jul. 2011.
- [9] M. F. Schubert, J. Xu, J. K. Kim, E. F. Schubert, M. H. Kim, S. Yoon, S. M. Lee, C. Sone, T. Sakong, and Y. Park, "Polarization-matched GaInN/AlGaInN multi-quantum-well light-emitting diodes with reduced efficiency droop," *Appl. Phys. Lett.*, vol. 93, no. 4, p. 041102, July 2008.
- [10] J. P. Liu, J.-H. Ryou, R. D. Dupuis, J. Han, G. D. Shen, and H. B. Wang, "Barrier effect on hole transport and carrier distribution in InGaN/GaN multiple quantum well visible light-emitting diodes," *Appl. Phys. Lett.*, vol. 93, no. 2, p. 021102, July 2008.
- [11] I. H. Brown, P. Blood, P. M. Smowton, J. D. Thomson, S. M. Olaizola, A. M. Fox, P. J. Parbrook, and W. W. Chow, "Time evolution of the screening of piezoelectric fields in InGaN quantum wells," *IEEE J. Quantum Electron.*, vol. 42, no. 12, pp. 1202–1208, Dec. 2006.
- [12] H. Zhao, R. A. Arif, and N. Tansu, "Design analysis of staggered InGaN quantum wells light-emitting diodes at 500–540 nm," *IEEE J. Sel. Top. Quantum Electron.*, vol. 15, no. 4, pp. 1104–1114, July/Aug. 2009.
- [13] R. A. Arif, Y. K. Ee, and N. Tansu, "Polarization engineering via staggered InGaN quantum wells for radiative efficiency enhancement of light emitting diodes," *Appl. Phys. Lett.*, vol. 91, no. 9, p. 091110, Aug. 2007.
- [14] C. T. Liao, M. C. Tsai, B. T. Liou, S. H. Yen, and Y. K. Kuo, "Improvement in output power of a 460 nm InGaN light-emitting diode using staggered quantum well," *J. Appl. Phys.*, vol. 108, p. 063107, 2010.
- [15] H. Zhao and N. Tansu, "Optical gain characteristics of staggered InGaN quantum wells lasers," *J. Appl. Phys.*, vol. 107, no. 11, p. 113110, June 2010.
- [16] S. H. Park, D. Ahn, and J. W. Kim, "High-efficiency staggered 530 nm InGaN/InGaN/GaN quantum-well light-emitting diodes," *Appl. Phys. Lett.*, vol. 94, no. 4, p. 041109, Jan. 2009.
- [17] R. A. Arif, H. Zhao, and N. Tansu, "Type-II InGaN-GaNAs quantum wells for lasers applications," *Appl. Phys. Lett.*, vol. 92, no. 1, p. 011104, Jan. 2008.
- [18] H. Zhao, R. A. Arif, and N. Tansu, "Self-consistent gain analysis of type-II 'W' InGaN-GaNAs quantum well lasers," *J. Appl. Phys.*, vol. 104, no. 4, p. 043104, Aug. 2008.
- [19] S. H. Park, Y. T. Lee, and J. Park, "Optical properties of type-II InGaN/GaAsN/GaN quantum wells," *Opt. Quantum Electron.*, vol. 41, no. 11–13, pp. 779–785, Nov. 2009.
- [20] J. Park and Y. Kawakami, "Photoluminescence property of InGaN single quantum well with embedded AlGaIn  $\delta$  layer," *Appl. Phys. Lett.*, vol. 88, no. 20, p. 202107, May 2006.
- [21] S. H. Park, J. Park, and E. Yoon, "Optical gain in InGaN/GaN quantum well structures with embedded AlGaIn  $\delta$  layer," *Appl. Phys. Lett.*, vol. 90, no. 2, p. 023508, Jan. 2007.
- [22] H. Zhao, R. A. Arif, Y. K. Ee, and N. Tansu, "Self-consistent analysis of strain-compensated InGaN-AlGaIn quantum wells for lasers and light-emitting diodes," *IEEE J. Quantum Electron.*, vol. 45, no. 1, pp. 66–78, Jan. 2009.
- [23] H. Zhao, G. Liu, and N. Tansu, "Analysis of InGaN-delta-InN quantum wells for light-emitting diodes," *Appl. Phys. Lett.*, vol. 97, no. 13, p. 131114, Oct. 2010.
- [24] Y. Li, B. Liu, R. Zhang, Z. Xie, and Y. Zheng, "Investigation of optical properties of InGaN-InN-InGaN/GaN quantum-well in the green spectral regime," *Physica E*, vol. 44, no. 4, pp. 821–825, Jan. 2012.
- [25] M. C. Y. Chan, E. M. T. Cheung, and E. H. Li, "A tunable blue light emission of InGaN/GaN quantum well through thermal interdiffusion," *Mater. Sci. Eng., B*, vol. 59, no. 1, pp. 283–287, May 1999.
- [26] M. D. McCluskey, L. T. Romano, B. S. Krusor, N. M. Johnson, T. Suski, and J. Jun, "Interdiffusion of In and Ga in InGaN quantum wells," *Appl. Phys. Lett.*, vol. 73, no. 9, pp. 1281–1283, July 1998.
- [27] C. C. Chuo, C. M. Lee, and J. I. Chyi, "Interdiffusion of In and Ga in InGaN/GaN multiple quantum wells," *Appl. Phys. Lett.*, vol. 78, no. 3, pp. 314–316, Nov. 2000.
- [28] B. S. Ooi, K. McIlvaney, M. W. Street, A. S. Helmy, S. G. Ayling, A. C. Bryce, J. H. Marsh, and J. S. Roberts, "Selective quantum-well intermixing in GaAs-AlGaAs structures using impurity-free vacancy diffusion," *IEEE J. Quantum Electron.*, vol. 33, pp. 1784–1793, 1997.
- [29] C. L. Tan, H. S. Djie, Y. Wang, C. E. Dimas, V. Hongpinyo, Y. H. Ding, and B. S. Ooi, "Wavelength tuning and emission width widening of ultrabroad quantum dash interband laser," *Appl. Phys. Lett.*, vol. 93, Sept. 2008, Art. 111101.
- [30] C. Chen, Y. Wang, C. L. Tan, H. S. Djie, B. S. Ooi, J. C. M. Hwang, G. T. Dang, and W. H. Chang, "Effects of intermixing on gain and alpha factors of quantum-dash lasers," *IEEE Photon. Technol. Lett.*, vol. 20, pp. 1654–1656, Sept.–Oct. 2008.
- [31] C. C. Chuo, C. M. Lee, T. E. Nee, and J. I. Chyi, "Effects of thermal annealing on the luminescence and structural properties of high indium-content InGaN/GaN quantum wells," *Appl. Phys. Lett.*, vol. 76, no. 26, pp. 3902–3904, May 2000.
- [32] S. L. Chuang and C. S. Chang, "k-p method for strained wurtzite semiconductors," *Phys. Rev. B*, vol. 54, no. 4, pp. 2491–2504, July 1996.
- [33] S. L. Chuang, "Optical gain of strained wurtzite GaN quantum-well lasers," *IEEE J. Quantum Electron.*, vol. 32, no. 10, pp. 1791–1800, Oct. 1996.
- [34] I. Vurgaftman and J. R. Meyer, "Band parameters for nitrogen-containing semiconductors," *J. Appl. Phys.*, vol. 94, no. 6, pp. 3675–3696, June 2003.
- [35] J. Crank, *Mathematics of Diffusion*. Oxford Univ. Press, Mar. 1980.
- [36] C.-C. Chen, T.-H. Hsueh, Y.-S. Ting, G.-C. Chi, and C.-A. Chang, "Effects of In and Ga interdiffusion on the optical gain of InGaN/GaN quantum well," *J. Appl. Phys.*, vol. 90, no. 10, pp. 5180–5182, Nov. 2001.

**Hongping Zhao** received the Bachelor's degree in physics from Nanjing Normal University (China) in 2003, the Master's degree in electrical engineering from Southeast University (China) in 2005, and the Ph.D. degree in electrical engineering from Lehigh University, Bethlehem, PA, USA, in 2011.

Since July 2011, she has been a tenure-tracked assistant professor in the Department of Electrical Engineering and Computer Science (EECS) at Case Western Reserve University. Her research areas cover device physics, epitaxial growth, and fabrication of semiconductor optoelectronics devices based on III-nitride semiconductor nanostructures. To date, she has been author or coauthor of more than 105 research publications in refereed international journals and conference proceedings. She is a regular reviewer of the leading journals in the areas of applied physics, quantum electronics, nanotechnology, photonics and optoelectronics.

Dr. Zhao is the recipient of the SPIE educational scholarship in optical science and engineering for 2008 and 2009. She has also served as a panel review member for National Science Foundation.

**Xuechen Jiao** received the B.S. degree in physics from Liaoning University in June 2009, and the M.S. degree in optics from Institute of Optics, Chinese Academy of Science in December 2011, and is currently pursuing the Ph.D. degree in physics at North Carolina State University.

From January 2012 to May 2012, he was research assistant in the Department of Electrical Engineering and Computer Science at Case Western Reserve University.

**Nelson Tansu** was born in 1977. He received the B.S. degree in applied mathematics, electrical engineering, and physics (with Highest Distinction) and the Ph.D. degree in electrical engineering/applied physics from the University of Wisconsin-Madison, Madison, WI, USA, in 1998 and 2003, respectively.

Since July 2003, he has been a faculty member in the Department of Electrical and Computer Engineering (ECE) and Center for Photonics and Nanoelectronics (CPN) at Lehigh University, Bethlehem, PA, USA, where he currently is the Class of 1961 Associate Professor (with tenure). He currently serves as Associate Editor for OSA Optical Materials Express (2010–present), Assistant/Associate Editor for Nanoscale Research Letters (2007–present), and Editor-in-Chief for Optics (2013–present). He has published in over 240 refereed international journals (92) and conference (150+) publications, and holds several U.S. patents (total > 10). He also regularly reviews leading journals in applied physics, quantum electronics, nanotechnology, photonics, and optoelectronics areas. Previously, he has given numerous lectures, seminars, and keynote and invited talks (total > 45) at universities, research institutions, and conferences in the Canada, Europe, and Asia. His research works cover both the theoretical and experimental aspects of the physics of semiconductor optoelectronics

materials and devices, the physics of low-dimensional semiconductor (nanos-structure), and MOCVD and device fabrications of III-Nitride and III-V-Nitride semiconductor optoelectronics devices on GaAs, InP, and GaN substrates.

Dr. Tansu served as the Primary Guest Editor of the IEEE JOURNAL OF SELECTED TOPICS IN QUANTUM ELECTRONICS (2008–2009) and IEEE/OSA JOURNAL OF DISPLAY TECHNOLOGY (2012–2013), and he also serves as an Associate Editor for IEEE PHOTONICS JOURNAL (2009–present). He served on the Technical Program Committee for several major technical conferences for IEEE, OSA, SPIE, and APS, including IEEE/OSA Conference on Lasers and Electro-Optics (2007–2009, 2013), SPIE Photonics West (2009–2013), APS March Annual Meeting (2007, 2009–2011), and ACP (2012, 2013), and others. He was selected as Invited General Participant at the 2008 National Academy of Engineering (NAE)'s U.S. Frontiers of Engineering (FOE) Symposium, and he served as the Organizing Committee for the 2009 NAE's U.S. Frontiers of Engineering Symposium. Recently, he has been invited to participate in the NAE's 2012 German-American Frontiers of Engineering Symposium (GAFOE).